Agricultural and Forest Meteorology 322 (2022) 109009

Contents lists available at ScienceDirect

Agricultural and Forest Meteorology

journal homepage: www.elsevier.com/locate/agrformet

# The probability distribution of absorbed direct, diffuse, and scattered radiation in plant canopies with varying structure

Brian N. Bailey [*,a], Kaiming Fu [a,b]

[a] Department of Plant Sciences, University of California, Davis, CA USA
[b] Department of Electrical and Computer Engineering, University of California, Davis, CA USA

ARTICLE INFO

*Keywords:*
Canopy structure
Leaf angle distribution
Plant canopy
Radiation

ABSTRACT

When applied to plant canopies, classical radiation theory for a turbid medium yields relatively simple expressions for average fluxes of absorbed radiation within an arbitrary volume of vegetation. However, due to the effects of shading and leaf angle, these averaging volumes usually contain a continuous distribution of leaf-level radiative fluxes ranging from full sun to full shade. These distributions are obscured within turbid media models and are thus usually not considered directly unless a computationally expensive leaf-resolving model is used. Consideration of the full probability distribution of absorbed radiative fluxes can yield valuable information about interactions between plant structure and function, not only for radiative fluxes but also for fluxes of radiation-dependent biophysical processes such as photosynthesis. This work presents the theoretical derivation of probability distributions of absorbed direct, diffuse, scattered, and total radiative fluxes for homogeneous canopies with varying structure. The theory is verified against predictions of a three-dimensional leaf-resolving model, and used to explore the impacts of canopy structure on the distribution of absorbed radiation.

## 1. Introduction

Over a half century ago, the landmark work of Monsi and Saeki (1953) (English translation provided in Monsi and Saeki, 2005) used the Beer–Lambert law to describe transmission of solar radiation through horizontally homogeneous plant canopies as a function of the cumulative leaf area index (LAI). The observed exponential decay in transmitted radiation with canopy depth can be derived from the radiative transfer equation by assuming that a canopy is analogous to a volume of radiatively participating gas or "turbid medium", along with assumptions that radiation is collimated and there is no emission or scattering in solar bands. This resulting simple exponential relationship effectively predicts cumulative transmission and absorption of radiation per unit ground area as a function of cumulative LAI, which can be used to estimate the average absorbed flux per unit leaf area. As solar radiation is the driver for essentially all biophysical processes in plant systems, these average fluxes can be used as the basis for prediction of numerous radiation-dependent processes such as photosynthesis, transpiration, microclimate, and many others. Consequently, the Beer–Lambert law is at the heart of nearly all plant systems models, including crop models (Jones and Leinonen, 2003; Keating et al., 2003), ecosystem models (Bonan et al., 2003; Krinner et al., 2005), and land surface models (Lawrence et al., 2019; Sellers et al., 1996).

The theory underpinning application of Beer–Lambert law in plant canopies has undergone substantial refinement in the years since the work of Monsi and Saeki (1953), including representation of anisotropy due to leaf orientation (Ross, 1981), diffuse solar radiation transfer (Goudriaan, 1977; Norman, 1979), scattering (Goudriaan, 1977; Norman, 1979), and heterogeneity/clumping (Bailey et al., 2020; Chen and Black, 1993). To represent vertical variation in radiation interception and its impact on dependent sub-processes, so-called "multilayer" models emerged that calculate fluxes over discrete layers of canopy (Bonan et al., 2021; Norman, 1979; Pyles et al., 2000). As computational capabilities increased, models with yet further detail arose in which Beer–Lambert law was applied to individual plant crowns (Cescatti, 1997; Wang and Jarvis, 1990), or sub-crown volumes usually called "voxels" (Bailey et al., 2014; Kimes and Kirchner, 1982; Sinoquet et al., 2001).

Turbid media models like those introduced above generally focus on modeling transmitted radiation, which can then be converted to average absorbed radiation fluxes per unit leaf area using the LAI and leaf absorptivity. Thus, regardless of the scale of discretization, turbid media

* Corresponding author.
*E-mail address:* bnbailey@ucdavis.edu (B.N. Bailey).

https://doi.org/10.1016/j.agrformet.2022.109009
Received 18 October 2021; Received in revised form 9 May 2022; Accepted 14 May 2022
Available online 25 May 2022

models yield average absorbed radiative fluxes over the discrete volume of interest (although it is possible to additionally partition average fluxes between sunlit and shaded leaf area in the volume; DePury and Farquhar, 1997; Wang and Leuning, 1998), which in turn can be used to determine average fluxes of radiation-dependent processes through substitution. However, within a volume of vegetation, leaf angle and shading typically create a continuous distribution of radiation flux values ranging from full sun to full shade that is obscured when only average fluxes are considered. Three-dimensional, leaf-resolving models are a recent innovation that enable the prediction of the full distribution of fluxes within an arbitrarily defined volume of vegetation (Bailey, 2019; Chelle and Andrieu, 1998; Cieslak et al., 2008). Their obvious drawback is the extremely high computational cost, which usually limits their application to the scale of a few plants.

This work extends classical plant radiative transfer theory to derive relatively simple expressions for the leaf-level probability distribution of absorbed direct, diffuse, and scattered radiation fluxes within horizontally homogeneous canopies. Rather than utilizing the traditional approach of aggregating these processes into average fluxes across some subset of the canopy volume (e.g., average over whole-canopy, canopy layers, sunlit or shaded leaves, leaf angle classes), we instead seek to derive the statistical distribution of such fluxes across the canopy. It is important here to distinguish between the probability distribution of transmitted or absorbed radiation fluxes per unit horizontal canopy area, and per unit leaf area. Transmission per unit canopy area can be described by Beer–Lamber law, from which absorption on a per unit canopy area basis can be readily calculated (absorption is the complementary of transmission). Theoretical approaches have been developed to describe the probability distribution of radiation transmission, but they are typically based on empirical statistical approaches that fit assumed distributions to measurements (Ross et al., 1998; Stenberg, 1995). However, it is the absorbed flux per unit leaf area, which is the focus of this work, that is most relevant to plant function as this is the flux actually received by the plant tissues and is the flux substituted into sub-models such as photosynthesis. Traditionally, the probability distribution of the absorbed flux has only been accessible through detailed 3D leaf-resolving simulations (e.g., Bailey, 2019).

Retaining the statistical distributions of absorbed fluxes rather than immediately aggregating into averages is valuable for several reasons. First, it provides a more informative description of these processes and the resulting effect of canopy structure. Much like other geophysical fields, flux distributions provide an insightful view into contributions of individuals to average emergent behavior, which is largely obscured by turbid-media-based canopy radiation transport models. Second, disaggregation into statistical distributions allows for more intuitive specification of variability in model parameters, since they can also be specified according to probability distributions rather than according to some arbitrary spatial delineation. Third, once the distribution of radiative fluxes is known, the radiation probability distribution can be substituted into dependent models such as the energy balance equation or a photosynthesis model to yield probability distributions for these processes. Finally, the theoretical probability distributions can serve as what is arguably the most rigorous verification test of leaf-resolving radiation absorption models currently available.

## 2. Theory

### 2.1. Radiation absorption kernel

#### 2.1.1. Direct radiation component

In order to derive the probability distribution of absorbed radiation for a canopy, we first consider absorption by a single layer of planar leaf elements illuminated by a collimated radiation source (i.e., no penumbral effects) with no self-shading. The orientation of each leaf is defined by the unit normal vector $\boldsymbol{\Omega}_L$ represented by spherical coordinates $\theta_L$ (zenith) and $\phi_L$ (azimuth), and follows a random inclination distribution that is independent of azimuthal direction. It is further assumed that radiative wavelengths are independent such that all radiative fluxes and surface properties can be defined as integrals over arbitrary wavebands. Initially, leaves are assumed to be black, and an extension to non-black leaves is given in Section 2.2.3.

Assuming perfect absorption, the absorbed radiation flux due to incident collimated solar radiation emanating from direction $\boldsymbol{\Omega}_s$ is

$$\begin{aligned} R_{L,dir} &= R_{i,dir}|\boldsymbol{\Omega}_L \cdot \boldsymbol{\Omega}_s| \\ &= R_{i,dir}|\sin\theta_s \sin\theta_L \cos\phi_L + \cos\theta_s \cos\theta_L|, \end{aligned} \tag{1}$$

where $R_{i,dir}$ is the incoming direct solar radiative flux on a plane perpendicular to the sun direction (thus, $0 \le R_{L,dir}/R_{i,dir} \le 1$), $\theta_s$ is the zenith angle of the solar direction, and by convention we arbitrarily take $\phi_L$ to be zero in the direction of the solar azimuth. Using the following triangle identity with angle $\gamma$ between orthogonal components $\cos\theta_s$ and $\sin\theta_s \cos\phi_L$

$$\sin\gamma = \frac{\cos\theta_s}{\sqrt{\sin^2\theta_s \cos^2\phi_L + \cos^2\theta_s}}, \tag{2}$$

$$\cos\gamma = \frac{\sin\theta_s \cos\phi_L}{\sqrt{\sin^2\theta_s \cos^2\phi_L + \cos^2\theta_s}}, \tag{3}$$

enables substitution into Eq. (1) to yield

$$R_{L,dir} = R_{i,dir}|\cos\gamma \sin\theta_L + \sin\gamma \cos\theta_L| \sqrt{\sin^2\theta_s \cos^2\phi_L + \cos^2\theta_s}. \tag{4}$$

Applying the additive angle identity gives

$$R_{L,dir} = R_{i,dir}|\sin(\theta_L + \gamma)| \sqrt{\sin^2\theta_s \cos^2\phi_L + \cos^2\theta_s}, \tag{5}$$

which can be explicitly solved for $\theta_L$ to give

$$\theta_L = \begin{cases} \sin^{-1}\left(\dfrac{R_{L,dir}}{R_{i,dir}\sqrt{\sin^2\theta_s \cos^2\phi_L + \cos^2\theta_s}}\right) - \gamma & \text{if } \theta_L \ge \gamma \\ \pi - \sin^{-1}\left(\dfrac{R_{L,dir}}{R_{i,dir}\sqrt{\sin^2\theta_s \cos^2\phi_L + \cos^2\theta_s}}\right) - \gamma & \text{otherwise.} \end{cases} \tag{6}$$

The leaf orientation distribution is described by the probability density function $g_L(\theta_L)$, and is subject to the normalization condition

$$\int_0^{\pi/2} g_L(\theta_L) d\theta_L = 1. \tag{7}$$

Note that following common convention, $g_L(\theta_L)$ has already been weighted by solid angle, and thus a factor of $\sin\theta_L$ is not included in the integrand but is instead wrapped within $g_L$.

We seek to derive the distribution of the probability that a leaf in the layer has a radiative flux equal to $R_{L,dir}$, which we term the direct radiation absorption kernel, $\kappa_{dir}$. This can be accomplished by performing a change of variables as follows

$$\kappa_{dir}\left(R_{L,dir}, R_{i,dir}\right) = \frac{1}{2\pi} \int_0^{2\pi} g_L\left(\theta_L\left(R_{L,dir}, R_{i,dir}\right)\right) \left|\frac{\partial\theta_L}{\partial R_{L,dir}}\right| d\phi_L. \tag{8}$$

Substituting the expression for $\theta_L$ given in Eq. (7) yields

$$\kappa_{dir}\left(R_{L,dir}, R_{i,dir}\right) = \frac{1}{2\pi} \int_0^{2\pi} \frac{g_L\left(\theta_L\left(R_{L,dir}, R_{i,dir}\right)\right)}{u\sqrt{1 - \left(R_{L,dir}/u\right)^2}} d\phi_L, \tag{9}$$

where $u = R_{i,dir}\sqrt{\sin^2\theta_s \cos^2\phi_L + \cos^2\theta_s}$, and the integrand is taken to

be zero when $u < R_{L,dir}$. For a single leaf layer, $R_{i,dir}$ is equal to the unobstructed direct solar radiation flux on a surface perpendicular to the sun direction, which we denote as $R_{0,dir}$. Note also that the average of the direct kernel is simply $G(\theta_s)\, R_{i,dir}$.

Eq. (10) cannot be readily integrated analytically, but can be integrated numerically. Computer code for performing this integration is provided in the manuscript's supplemental material.

The advantage of the above formulation is that it can be used to calculate the probability at a single value of $R_{L,dir}$. However, when calculating a discrete probability distribution, it is often easier to use an alternative approach. First, $R_{L,dir}(\theta_L, \phi_L)$ can be calculated on a uniform discrete spherical grid. The corresponding bin in the discrete $\kappa_{dir}$ distribution can then be determined for each of these calculated $R_{L,dir}(\theta_L, \phi_L)$ values and weighted by $g_L(\theta_L)$ at each of these points to determine the probability in each discrete bin. Examples of both methods for calculating $\kappa_{dir}$ are provided in the computer code in the manuscript's supplemental material.

#### 2.1.2. Diffuse radiation component

Considering the same leaf layer as above, the diffuse component of the absorbed solar radiation flux on an individual leaf in the layer is given by

$$R_{L,diff} = \frac{1}{\pi} \int_0^{2\pi} \int_0^{\pi/2} R_{i,diff} |\sin\theta_d \sin\theta_L \cos(\phi_L - \phi_d) + \cos\theta_d \cos\theta_L| \sin\theta_d \, d\theta_d d\phi_d, \tag{10}$$

where $\theta_d$ and $\phi_d$ are respectively zenith and azimuth angles in the upper hemisphere. $R_{i,diff}$ is the diffuse component of the directional unobstructed radiation flux, which is equal to $R_{0,diff} f_d(\theta_d, \phi_d)$ for a single leaf layer, where $R_{0,diff}$ is the unobstructed diffuse radiation flux on a horizontal surface, and $f_d(\theta_d, \phi_d)$ describes the directional distribution of incoming diffuse solar radiation across the upper hemisphere, and is subject to the normalization condition of

$$\frac{1}{\pi} \int_0^{2\pi} \int_0^{\pi/2} f_d(\theta_d, \phi_d) \cos\theta_d \sin\theta_d \, d\theta_d d\phi_d = 1. \tag{11}$$

Applying the method of transformations, the absorption kernel for diffuse radiation is given by

$$\frac{1}{\pi} \int_0^{2\pi} \int_0^{\pi/2} f_d(\theta_d, \phi_d) \cos\theta_d \sin\theta_d \, d\theta_d d\phi_d = 1. \tag{12}$$

In general, an analytical solution for $\kappa_{diff}$ does not exist and must be computed numerically. Computer code for doing so is provided in the manuscript's supplemental material.

If the directional diffuse radiation flux is uniform across the sky (e.g., a uniform overcast sky), $f_d = 1$, and $R_{L,diff} = R_{0,diff}$. In this case, the radiation absorption kernel is trivial and is given by a $\delta$ distribution with a peak at $R_{L,diff}/R_{0,diff} = 1$

$$\kappa_{diff}\left(R_{L,diff}, R_{i,diff}\right) = \delta\left(R_{L,diff} - R_{i,diff}\right). \tag{13}$$

### 2.2. Whole-canopy radiation probability distribution

#### 2.2.1. Direct radiation component

Expressions for the direct and diffuse radiation absorption kernel have been derived above, which contain canopy structure information corresponding to leaf orientation only. For a canopy of multiple layers, the leaf area distribution is an additional structural attribute that augments the absorbed radiation distribution through shading. This means that the flux incident on a given leaf $R_i$ is no longer equal to $R_{0,dir}$ (or $(R_{0,diff} \cdot f_d)$ for diffuse radiation). Thus, the basic approach for calculating the absorbed radiation distribution for a whole canopy is to calculate the incident radiation flux field at a given depth in the canopy, substitute that value for $R_i$, and integrate over the canopy depth.

In order to derive whole-canopy absorption distributions, consider a homogeneous canopy with leaves randomly oriented according to the azimuthally isotropic distribution $g_L(\theta_L)$. The density of leaf elements in a column of canopy volume is defined by the cumulative downward leaf area index (LAI) $L$, which is zero at the canopy top and equal to the one-sided leaf surface area per unit horizontal canopy area $L_c$ at the canopy bottom.

The average flux of incoming (transmitted) direct radiation at a depth of $L$ is given by

$$R_{i,dir}(L; \theta_s) = R_{0,dir} \exp\left( -\frac{G(\theta_s) L}{\cos\theta_s} \right), \tag{14}$$

where $G$ is the fraction of leaf area projected in the direction of the sun direction $\theta_s$ and is defined mathematically as

$$G(\theta_s) = \frac{1}{2\pi} \int_0^{2\pi} \int_0^{\pi/2} g_L(\theta_L) |\sin\theta_s \sin\theta_L \cos\phi_L + \cos\theta_s \cos\theta_L| \, d\theta_L \, d\phi_L, \tag{15}$$

where it is reminded that $\phi_L$ is taken to be zero at the solar azimuth angle.

The PDF of absorbed direct radiation for sunlit leaf area, $P_{c,sun}$, is

$$P_{c,sun}\left(R_{L,dir}\right) = \frac{1}{L_c} \int_0^{L_c} \kappa_{dir}\left(R_{L,dir},\, R_{i,dir}\right) dL, \tag{16}$$

where $R_{i,dir}$ is given by Eq. (15).

Since, for direct radiation, the absorption kernel is independent of height/LAI, and noting that the whole-canopy sunlit leaf area fraction is

$$\begin{aligned} f_{sun} &= \frac{1}{L_c} \int_0^{L_c} \exp\left( -\frac{GL}{\cos\theta_s} \right) dL \\ &= \frac{\cos\theta_s}{GL_c} \left[ 1 - \exp\left( -\frac{GL_c}{\cos\theta_s} \right) \right], \end{aligned} \tag{17}$$

we arrive at

$$P_{c,sun}\left(R_{L,dir}\right) = \kappa_{dir}\left(R_{L,dir}, R_{0,dir}\right) f_{sun}. \tag{18}$$

Given that the PDF of the shaded leaf area is a $\delta$ function at $R_{L,dir} = 0$ with an integrated probability of $1 - f_{sun}$, the whole-canopy PDF for absorbed direct radiation, $P_{c,dir}$, is

$$P_{c,dir}\left(R_{L,dir}\right) = \kappa_{dir}\left(R_{L,dir}, R_{0,dir}\right) f_{sun} + \delta\left(R_{L,dir}\right)(1 - f_{sun}). \tag{19}$$

#### 2.2.2. Diffuse radiation component

The average flux of incoming (transmitted) diffuse radiation in direction $\boldsymbol{\Omega}_d$ and arbitrary depth into the canopy of $L$ is

$$R_{i,diff}(L; \theta_d, \phi_d) = R_{0,diff} f_d(\theta_d, \phi_d) \exp\left( -\frac{G(\theta_d) L}{\cos\theta_d} \right). \tag{20}$$

The absorption kernel evaluated at $R_{i,diff}$ can be integrated with respect to $L$ to give the PDF of absorbed diffuse radiation over the canopy depth

$$P_{c,diff}\left(R_{L,diff}\right) = \frac{1}{L_c} \int_0^{L_c} \kappa_{diff}\left(R_{L,diff},\, R_{i,diff}\right) dL. \tag{21}$$

Since the diffuse absorption kernel depends on height (and thus $L$), the kernel must be re-calculated at each depth during integration over $L$ according to the local value of $R_{i,diff}$.

#### 2.2.3. Radiation scattering

The above analysis assumed that all elements in the canopy are

black, meaning that all incident radiation is absorbed. For the photosynthetically active portion of the solar radiation spectrum (wavelengths of approximately 400–700 nm), plant leaves typically absorb around 80–90% of incident radiation (Jones and Vaughan, 2010), and thus the assumption of black leaves may be a reasonable first approximation in many applications. However, for near-infrared solar radiation (wavelengths $\gtrsim$700 nm), plants generally only absorb around 20% of incident radiation, with roughly the remaining 40% reflected and 40% transmitted (Jones and Vaughan, 2010). Thus, in the near-infrared band, which carries about half of total incident solar radiative energy, scattering is likely to be important in many applications.

In order to derive the distribution of absorbed scattered radiation, we need a means for calculating the scattered radiation intensity. Simple analytical expressions for scattered intensity are not available in general. Most 1D canopy models use highly simplified schemes for radiation scattering (e.g., Norman, 1979), but caution should be exercised when using these schemes because they are not explicitly consistent with the equations of radiative transfer. In this work, a numerical solution to the radiative transfer equation (RTE) is used to determine the incoming radiation field on a leaf layer when scattering is considered. Derivation of a simple 1D model for the scattered intensity is given in Appendix A.

The scattered radiation flux absorbed by a leaf at depth $L$ is

$$R_{L,sc}(L,\boldsymbol{\Omega}_L) = \frac{1-\rho_L-\tau_L}{2\pi}\int_{4\pi} I_s(L,\boldsymbol{\Omega})\,|\boldsymbol{\Omega}_L\cdot\boldsymbol{\Omega}|\cos\theta_s\,d\Omega, \tag{22}$$

where $\rho_L$ and $\tau_L$ are respectively the leaf reflectivity and transmissivity, and $I_s(L;\boldsymbol{\Omega}_L)$ is the incoming scattered radiation intensity (see Appendix A).

It is not possible to calculate a generalized absorption kernel for scattered radiation because the angular distribution of the scattered radiation intensity varies with height. However, the distribution of absorbed scattered radiation can be calculated in a single step using Eq. (24) and a change of variables similar to that of direct and diffuse radiation

$$P_{c,sc}(R_{L,sc}) = \frac{1}{2\pi L_c}\int_0^{L_c}\int_0^{2\pi} g_L(\theta_L(R_{L,sc}))\left|\frac{\partial\theta_L}{\partial R_{L,sc}}\right| d\phi\,dL. \tag{23}$$

#### 2.2.4. Convolution of direct, diffuse, and scattered distributions

The probability distribution of total absorbed solar radiation due to direct and diffuse components can be calculated through convolution of the two probability distributions

$$P_c(R_L) = \left(P_{c,dir} * P_{c,diff}\right)(R_L) = \int_0^{R_0} P_{c,dir}(x)\,P_{c,diff}(R_L-x)\,dx, \tag{24}$$

where $P_c(R_L)$ is the probability distribution of total absorbed radiation across all leaves in the canopy, $R_0 = R_{0,dir} + R_{0,diff}$ is the sum of the above-canopy direct and diffuse radiation fluxes on a horizontal surface. The incoming diffuse radiation fraction is defined by $f_{diff} = R_{0,diff}/R_0$. Similarly, if scattering is included, the total probability distribution can be calculated by performing another convolution with $P_{c,sc}$.

An alternative approach can also be used to calculate $P_c$ that is more efficient in most cases. Rather than dividing into direct and diffuse components, leaf area can be divided into sunlit and shaded fractions, with the total radiation flux calculated for each in a single step. This avoids convolution because the distributions for sunlit and shaded leaf area can simply be added together because they correspond to separate leaf area rather than separate fluxes incident on the same leaf area. For sunlit leaf area, $R_L(\theta_L,\phi_L)$ is calculated based on the sum of $R_{L,dir}(\theta_L,\phi_L)$ (Eq. (1)) and $R_{L,diff}(\theta_L,\phi_L)$ (Eq. (11)). The probability distribution for sunlit leaf area $P_{c,sun}(R_L)$ can be calculated similarly as before based on the total $R_L(\theta_L,\phi_L)$, except that it should be normalized such that

$$\int_0^{R_0} P_{c,sun}(R_L)\,dR_L = f_{sun}. \tag{25}$$

For shaded leaf area, $R_L(\theta_L,\phi_L)$ is calculated based only on $R_{L,diff}(\theta_L,\phi_L)$, and the calculated shaded leaf area distribution $P_{c,sh}(R_L)$ should integrate to $1-f_{sun}$. Finally, the total distribution $P_c(R_L)$ is simply the sum of $P_{c,sun}(R_L)$ and $P_{c,sh}(R_L)$.

### 2.3. Generalization to heterogeneous canopies

The above derivations focused on spatially homogeneous canopies for simplicity, but extension to vertically or horizontally homogeneous canopies is straight forward provided that the incoming radiation field can be readily calculated at any point.

Vertically-varying leaf angle distribution: if the canopy contains vertical regions with different leaf angle distributions, the absorption kernel must be calculated for each leaf angle distribution. Assuming that that the canopy still has homogeneous leaf area density and the leaf angle distribution is horizontally homogeneous, the appropriate kernel $\kappa_{dir}$ can be inserted in the integral of Eq. (17) (and analogously for Eqs. (23) and (25)), where it is noted that $\kappa_{dir}$ is now a function of height (or in this case LAI). Note also that $G(\theta)$ is also now a function of height, which should be considered in the calculation of $R_{i,dir}$. If discrete vertical zones of constant leaf angle distributions can be delineated, then the appropriate $\kappa_{dir}$ can be queried during numerical integration across discrete vertical levels. Alternatively, a generalized leaf angle distribution function $g_L$ based on one or more continuous parameters could be used (e.g., Campbell, 1986; Goel and Strebel, 1984), where the distribution shape parameters could be specified as a continuous function of height.

Variable leaf area density: if leaf area density varies with height only, the integrand in Eqs. (17), (23), and (25) becomes weighted by the leaf area density in each vertical layer increment in the integration. When leaf area density is vertically constant, the integration over height effectively becomes an equal-weighted average of the kernel over height, but with variable leaf area density it becomes an average weighted by layer leaf area density, e.g., Eq. (17) can be written as

$$P_{c,sun} = \frac{1}{L_c}\int_0^h \kappa_{dir}\left(R_{L,dir},R_{i,dir}\right)a(z)\,dz, \tag{26}$$

where $a(z)$ is the leaf area density at height $z$ (one-sided leaf area per unit volume of canopy), and $h$ is the canopy height. Similarly, if leaf area density varies three-dimensionally in space (e.g., a row crop, a savanna), the integral is performed over each spatial coordinate. This also requires calculation of the incoming radiation field, which in general requires a 3D turbid media radiation transfer model (e.g., Bailey et al., 2014; Kimes and Kirchner, 1982).

It is noteworthy that Eq. (28) can still be written as $P_{c,sun} = \kappa_{dir} f_{sun}$, and thus heterogeneity does not impact the probability distribution of absorbed direct radiation for sunlit leaf area, but only the relative weighting between sunlit and shaded leaf area. Thus, as long as $\kappa_{dir}$ is homogeneous, relatively simple, heterogeneous radiation models (e.g., Bailey et al., 2020) can be used to estimate the bulk canopy $f_{sun}$ and calculate $P_{c,sun}$.

### 2.4. Generalization to asymmetric or non-planar leaves

In the above analysis, absorbed radiative fluxes were calculated on a one-sided area basis assuming that each side of the leaf is radiatively symmetric. However, in instances where leaves are thick or non-planar (e.g., needles), it may be desirable to calculate the absorbed radiation PDF separately for each side of the leaf, or for all outward-facing surface normals considering only one-sided absorption. The above analysis can

be readily extended to such cases. One approach is to explicitly consider the direction of incident radiation and the leaf/surface normal direction. For example, in Eqs. (1) and (11), we took the absolute value of the dot product between the surface normal and radiation direction, thus effectively treating each side of the leaf symmetrically. To calculate the PDF over only upward surface normals, only the cases in which $\Omega_L \cdot \Omega_s > 0$ (or $\Omega_L \cdot \Omega_d > 0$ in the case of diffuse radiation) would be considered during integration. The flux incident on downward surface normals could also be separately calculated by considering only cases when the dot product is negative.

## 3. Test cases

Validating the above theory against direct experimental observations would be exceedingly difficult, as it would require a very large number of radiation measurements throughout the entire canopy depth at random angles following the canopy leaf angle distribution. It would also likely prohibit separation of direct, diffuse, and scattered components of the radiation flux, and potentially contain effects of clumping. In relatively rare cases (e.g., Baldocchi et al., 1986; Giuliani et al., 2000; Ross et al., 1998; Vesala et al., 2000), the probability distribution of the transmitted radiation flux has been reported based on experimental measurements, but this involves measurement at one angle (horizontal) and at often only one height (canopy bottom). Even if the measurements could feasibly be collected, it is probable that errors in the experiments would be comparable in magnitude to those of the model.

Because of the challenges inherent in direct experimental validation, the above theory was instead verified by comparing against PDFs generated from a 3D, leaf-resolving radiation transfer model. The overall approach was to adjust various settings in the 3D model to match several assumptions that were made in the derivation of the PDFs such as canopy homogeneity and collimated radiation, which allows for testing of the underlying theory for analytical generation of the PDFs. Major underlying differences between the analytical- and 3D-model-generated PDFs are that the canopy geometry is fully resolved in the 3D model, whereas the simplified approach above uses statistical transformations to estimate the absorption kernel along with assumptions of a turbid media to generate the whole-canopy PDFs.

The ray-tracing-based model of Bailey (2018) as implemented in the Helios modeling framework (Bailey, 2019) was used to simulate leaf-level PDFs of absorbed direct, diffuse, and scattered radiation fluxes. The model uses a reverse ray-tracing method that ensures adequate ray sampling for every geometric element. For simplicity, leaves are represented by a 25 × 25 grid of square patches of size 0.1 × 0.1 $m^2$. Bailey and Kent (2021) showed that a resolution of about 15 × 15 elements/leaf is adequate for representing radiation PDFs, but higher resolution was used in this work to minimize effects of element-scale averaging as much as possible.

Three-dimensional homogeneous canopies were generated with an LAI of 1.0 and different leaf angle distributions. The horizontal extent of the canopy was 10 × 10 $m^2$, and had periodic horizontal boundary conditions. Based on this geometry, the simulated canopy had about 10,000 leaves with 6.25 M total geometric elements. Four canonical leaf angle distributions were simulated: spherical, uniform, planophile, and erectophile (de Wit, 1965). The erectophile distribution has leaves that tend more toward vertical on average, and uniform and planophile have leaves tending more toward horizontal. The spherical distribution is isotropic, meaning that leaves have no preferred orientation and thus the rate of radiation attenuation is independent of direction. The equations used to calculated $g_L(\theta)$ for each of the leaf angle distributions is given in Table 2 of Bailey and Kent (2021).

Direct solar radiation was assumed to be collimated (no penumbral effects) following the assumption made in the analysis above, which was sampled using 11000 rays/element (625,000 rays/leaf). Four different solar zenith angles were simulated: 0, $25^{\circ}$, $50^{\circ}$, and $75^{\circ}$. Diffuse solar radiation was sampled using 10,000 rays/element (6.25 M rays/leaf). Cases were simulated in which leaves were black, and with leaf reflectivity and transmisitivity of $\rho_L = 0.25$ and $\tau_L = 0.25$. The ground was black for all simulations. When scattering was included, three scattering iterations were used in the 3D radiation model (cf. Bailey, 2018).

In order to explore the effect of the angular distribution of incoming diffuse radiation, a model was used to specify the diffuse angular distribution as a function of a single parameter. The normalized angular distribution of incoming diffuse radiation was calculated as (Harrison and Coombes, 1988)

$$f_d(\theta, \phi) = f_0 \Psi^{-K}, \tag{27}$$

where

$$\Psi = \cos^{-1}(\cos\theta_s \cos\theta + \sin\theta_s \sin\theta \cos(\phi - \phi_s)), \tag{28}$$

$f_0$ is a normalization factor that enforces the relationship

$$\frac{1}{\pi} \int_0^{2\pi} \int_0^{\pi/2} f_d(\theta, \phi) \cos\theta \sin\theta \, d\theta \, d\phi = 1, \tag{29}$$

and $K$ is an anisotropy factor. If $K = 0$, the diffuse radiation is isotropic, and as $K$ becomes large diffuse radiation becomes increasingly concentrated in the direction of the sun. Cases were run with $K = 0$, 0.5, and 1.0.

A visualization of the simulated canopy for one example case, along with the resulting canopy-level PDF of absorbed radiation flux, is shown in Fig. 1.

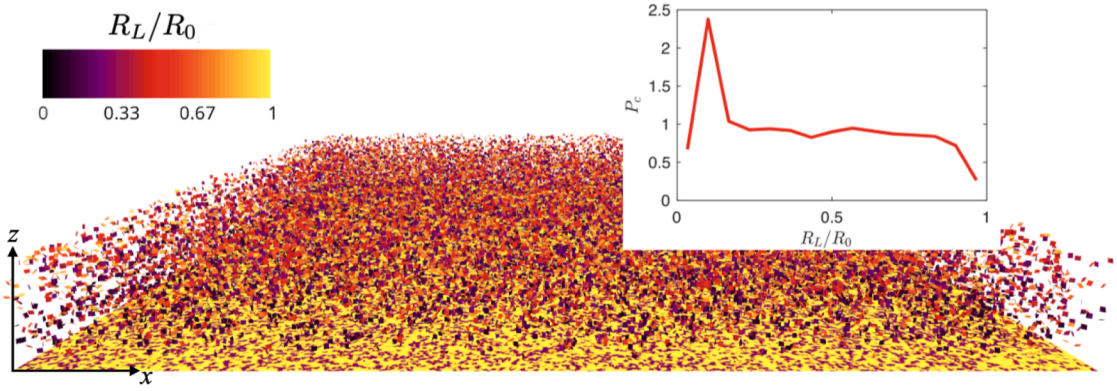


**Fig. 1.** Visualization of the absorbed radiation flux $R_L/R_0$ for the 3D simulation case with spherical leaf angle distribution, $\theta_s = 0$, $f_{diff} = 0.2$, and $K = 0$. Every leaf surface in the simulated canopy is visualized according to its position and orientation, and the surface is colored according to a pseudocolor mapping based on its absorbed radiation flux (see colorbar). The sub-axes show the resulting discrete probability distribution of absorbed radiation flux $P_c(R_L/R_0)$.

## 4. Results and discussion

### 4.1. Direct absorption kernel

Fig. 2 shows the direct radiation absorption kernel function, $\kappa_{dir}$ for spherical, uniform, planophile, and erectophile leaf angle distributions at solar zenith angles, $\theta_s$, of 0, 25°, 50°, and 75°. The spherical distribution produces a uniform distribution of absorbed radiation flux, since this distribution is uniform with respect to $\theta_L$ when weighted by solid angle. The spherical distribution corresponds to a state of minimum entropy in the radiation distribution, and any deviation from this random distribution creates an increase in entropy (Bailey and Kent, 2021). The "uniform" distribution has leaf angles that tend toward horizontal, which is due to the fact that solid angles decrease near the poles in a spherical coordinate system, and thus when weighted by solid angle the uniform distribution yields more leaves closer to horizontal. This produces a high probability of normalized radiation fluxes near 1 when the sun is directly overhead ($\theta_s = 0$). This peak in $R_{L,dir}/R_{0,dir}$ shifts toward lower values as solar zenith increases, where this peak value corresponds to the value of $R_{L,dir}/R_{0,dir}$ for a horizontal leaf. Similar behavior is created by the planophile distribution, which has leaf angles even more heavily biased toward horizontal. Because of this stronger bias toward horizontal leaves in the planophile distribution, peak values in the probability distribution are larger, with probabilities decaying more rapidly away from the peak. The erectophile distribution, which has leaf angles tending toward vertical, has a depression in the probability distribution around $R_{L,dir}/R_{0,dir} = 1$ when the sun is vertical. When the sun nears the horizon, there is a transition in the distribution in which a peak in probability forms at $R_{L,dir}/R_{0,dir} = 1$.

Agreement between the theoretical direct absorption kernel and that obtained by 3D simulation was excellent, with little if any deviation between the two. This suggested that the theory was correctly derived, and that there were a sufficient number of statistical leaf samples in the simulations.

### 4.2. Diffuse absorption kernel

Fig. 3 shows the diffuse radiation absorption kernel, $\kappa_{diff}$, for the four different leaf angle distributions and three different incoming diffuse radiation distributions with varying anisotropy. When incoming diffuse radiation is isotropic (i.e., $K = 0$), the diffuse radiation kernel is a $\delta$ function with a peak at $R_{L,diff}/R_{0,diff} = 1$ regardless of the leaf angle distribution. Since the incoming radiation flux is isotropic for this case, this also means that the absorbed radiation flux will be independent of leaf angle (provided that the surface can absorb radiation from both sides). As a result, the kernel is unaffected by leaf angle distribution when $K = 0$.

As the incoming diffuse radiation distribution becomes increasingly anisotropic and concentrated toward the vertical (i.e., increasing $K$), the diffuse absorption kernel generally includes a wider range of flux values. For leaf angle distributions that tend toward horizontal, the peak in the kernel tends to be located at high flux values, whereas the peak shifts toward smaller flux values as the leaf angle distribution shifts toward having more vertical leaves. The uniform leaf angle distribution creates a bimodal distribution with two peaks at opposite ends of the probability distribution.

As with the direct absorption kernel, there was very close agreement between the theoretical kernel and the kernel obtained from 3D simulation. This result confirms both the theoretical and 3D simulation approaches for calculation of absorbed diffuse radiation with no mutual leaf shading.

### 4.3. Direct whole-canopy absorption PDF

Fig. 4 shows the whole-canopy direct radiation absorption distribution, $P_{c,dir}$, for a horizontally homogeneous canopy of $LAI = 1$ for the four different leaf angle distributions and solar zenith angles. The most notable difference between the whole-canopy distribution and the corresponding kernel is the presence of the strong peak in the distribution at

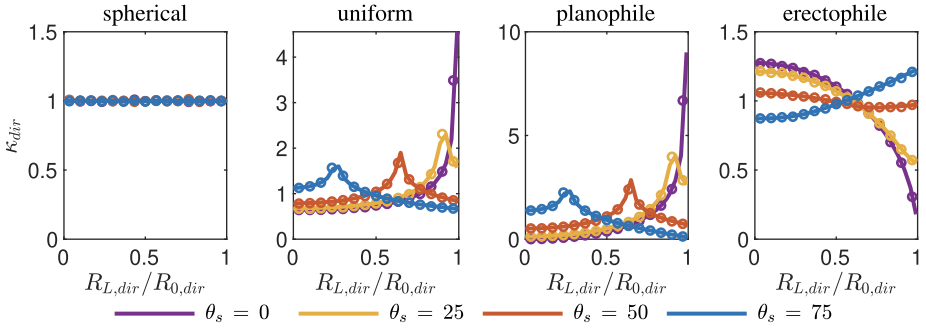


**Fig. 2.** Direct radiation absorption kernel: probability density function of absorbed direct radiation flux over a single layer of inclined leaves with no self-shading. The absorbed direct radiation flux, $R_{L,dir}$, is normalized by the incoming direct radiation flux on a surface perpendicular to the sun direction, $R_{0,dir}$. Azimuthally isotropic leaf angle distributions of spherical, uniform, planophile, and erectophile are shown in each pane as indicated by the title. Each line corresponds to a different solar zenith angle. Open symbols correspond to the kernel obtained from 3D simulation.

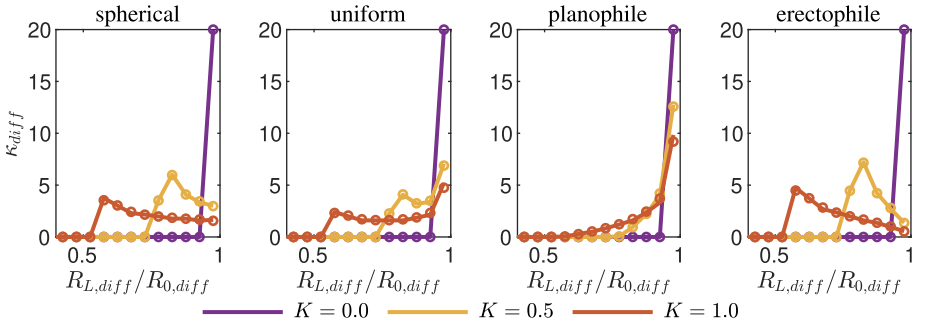


**Fig. 3.** Diffuse radiation absorption kernel: probability density function of absorbed direct radiation flux over a single layer of inclined leaves with no self-shading. The absorbed diffuse radiation flux, $R_{L,diff}$, is normalized by the incoming diffuse radiation flux on a horizontal surface, $R_{0,diff}$. Azimuthally isotropic leaf angle distributions of spherical, uniform, planophile, and erectophile are shown in each pane as indicated by the title. Each line corresponds to a different angular distribution of incoming diffuse radiation (see Eq. (29)). Open symbols correspond to the kernel obtained from 3D simulation. In all cases shown, the solar zenith angle was 0 (vertical).

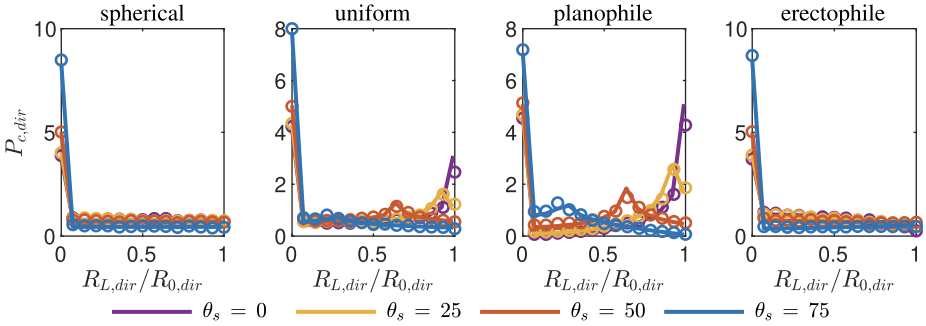


**Fig. 4.** Probability density function of absorbed direct radiation flux within a horizontally homogeneous canopy of $LAI = 1$. The absorbed direct radiation flux, $R_{L,dir}$, is normalized by the incoming direct radiation flux on a surface perpendicular to the sun direction, $R_{0,dir}$. Azimuthally isotropic leaf angle distributions of spherical, uniform, planophile, and erectophile are shown in each pane as indicated by the title. Each line corresponds to a different solar zenith angle. Open symbols correspond to the distribution obtained from 3D simulation.

$R_{L,dir}/R_{0,dir} = 0$. This peak corresponds to shaded leaf area, which in the case of no diffuse or scattered radiation, has an absorbed radiation flux of 0. As the projected leaf area in the direction of the sun increases, the fraction of shaded leaf area increases and thus the magnitude of the lower peak increases relative to the rest of the distribution.

Notably, the presence of a canopy (and thus shading) has no effect on the shape of the distribution for $R_{L,dir}/R_{0,dir} > 0$. The $R_{L,dir}/R_{0,dir} > 0$ portion of the distribution corresponds to sunlit leaf area, and thus there is no effect of surrounding leaves on its radiation distribution. Thus, the absorption distribution for sunlit leaf area is only determined by the absorption kernel $\kappa_{dir}$.

Agreement between the theoretical and 3D simulated distributions of absorbed direct radiation was very high. There was marginally lower agreement than for the absorption kernel alone, which was likely due to the strong peak in the distribution created by shaded leaf area that is difficult to perfectly resolve using a discrete probability distribution.

### 4.4. Diffuse whole-canopy absorption PDF

Fig. 5 shows the whole-canopy diffuse radiation absorption distribution, $P_{c,diff}$, for the four leaf angle distributions and levels of incoming radiation anisotropy. The overall shape of the distribution was very similar regardless of the leaf angle distribution or level of anisotropy in ambient diffuse radiation. There was a peak in the distribution near a value of $R_{L,diff}/R_{0,diff} = \exp(-k_d L)$ ($k_d$ being the diffuse attenuation coefficient), with a rapid decrease to the left of this peak and a more gradual decrease to the right. Increasing fraction of leaf area projected in the vertical direction or increasing $LAI$ (not shown) tends to shift the extent of the non-zero portion of the distribution to the left because it increases shading and thus increases the probability of having leaves with low radiative fluxes. It is perhaps surprising that the degree of anisotropy had a weak effect on the whole-canopy distribution, but had a strong effect on the diffuse distribution for a single layer of leaves with no shading (Fig. 3). This was also generally the case for the effect of leaf angle distribution.

Overall agreement between the theoretical and 3D simulated distributions was high, with differences between the two only slightly larger than that of the direct absorption distribution, $P_{c,dir}$. Differences tended to increase with increasing $K$ or as the leaf angle distribution tended toward horizontal, particularly near the peak in the distribution. It is possible that the 3D model tends to slightly smooth the peak in the distribution due to sub-leaf-scale flux averaging. However, these differences were overall fairly small.

### 4.5. PDF of scattered radiation

Fig. 6 shows the whole-canopy scattered radiation absorption distribution, $P_{c,sc}$, for the four leaf angle distributions and solar zenith angles. In all cases, the distribution appears roughly bell-shaped, with relatively small skewness and a peak near the middle of the distribution. For leaf angle distributions tending more toward horizontal, the deviation in the distribution appeared to decrease in general. The distribution shifted to the left as the solar zenith angle increased, which was more pronounced for distributions with higher probability of horizontal leaves.

Agreement between the theoretical and 3D simulated scattered distributions was relatively good considering the small scattered fluxes $R_{L,sc}$ relative to $R_{0,dir}$. Errors appeared to increase with solar zenith angle (which decreased the magnitude of scattered fluxes), and as the leaf angle distribution tended more toward horizontal. Because of the sharp gradients in the PDF, small errors can appear amplified in the discrete distribution.

### 4.6. Total absorption PDF

Example convolutions of direct and diffuse absorption PDFs are given in Fig. 7 for the uniform leaf angle distributions and various diffuse incoming radiation fractions. Addition of diffuse radiation tends to decrease the probability of leaves with very low radiation fluxes, and tends to remove the peak in probability at $R_L = 0$ that is observed in the direct radiation distributions due to shaded leaf area. As is to be expected, this effect became stronger as $f_{diff}$ is increased. In the case of $f_{diff} = 0$, the distribution will simply resemble that shown in Fig. 4 where all radiation was direct, and in the case of $f_{diff} = 1$ the distribution will resemble that shown in Fig. 5 where all radiation was diffuse. Intermediate values of $f_{diff}$ essentially produce a smooth transition

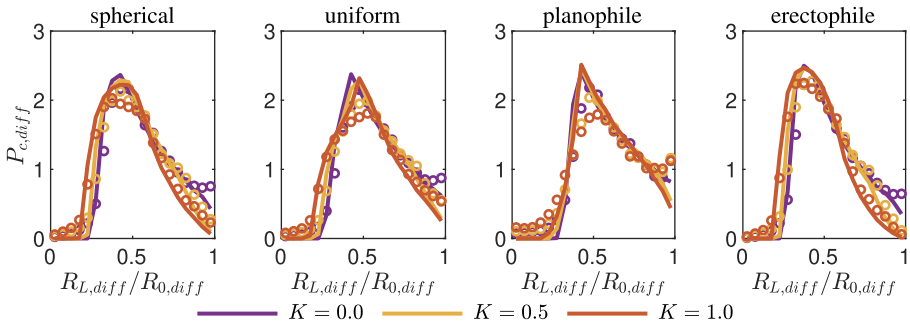


**Fig. 5.** Probability density function of absorbed diffuse radiation flux within a horizontally homogeneous canopy of $LAI = 1$. The absorbed diffuse radiation flux, $R_{L,diff}$, is normalized by the incoming diffuse radiation flux on a horizontal surface, $R_{0,diff}$. Azimuthally isotropic leaf angle distributions of spherical, uniform, planophile, and erectophile are shown in each pane as indicated by the title. Each line corresponds to a different angular distribution of incoming diffuse radiation (see Eq. (29)). Open symbols correspond to the distribution obtained from 3D simulation. In all cases shown, the solar zenith angle was 0 (vertical).

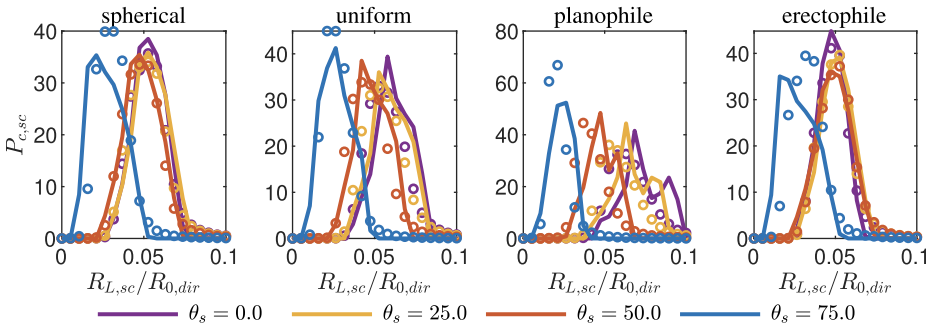


**Fig. 6.** Probability density function of absorbed scattered radiation flux within a horizontally homogeneous canopy of $LAI = 1$. Azimuthally isotropic leaf angle distributions of spherical, uniform, planophile, and erectophile are shown in each pane as indicated by the title. Each line corresponds to a different solar zenith angle. Open symbols correspond to the distribution obtained from 3D simulation. In all cases, the diffuse radiation fraction was $f_{diff} = 0$.

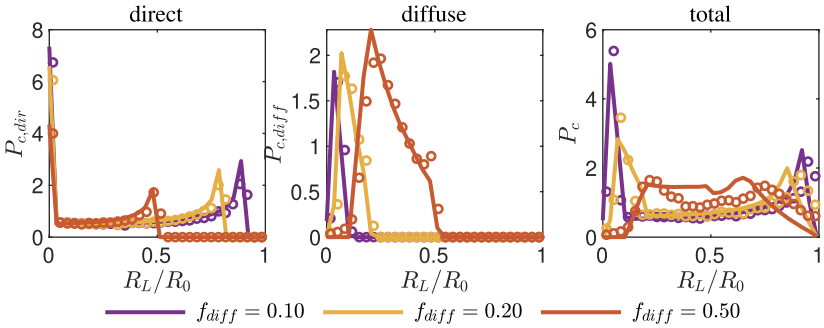


**Fig. 7.** Probability density function of absorbed direct radiation (left pane), diffuse radiation (middle pane), and sum of direct and diffuse radiation (right pane) within a horizontally homogeneous canopy of $LAI = 1$. Each line corresponds to a different incoming diffuse radiation fraction. Open symbols correspond to the distribution obtained from 3D simulation. In all cases shown, the solar zenith angle was 0 (vertical), the leaf angle distribution was uniform, and $K = 0$ (isotropic incoming diffuse radiation).

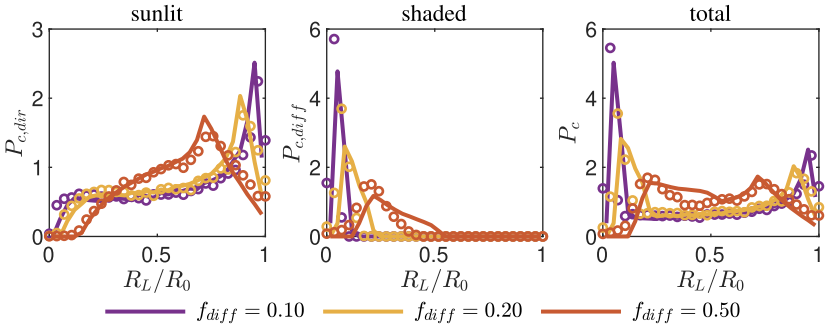


**Fig. 8.** Probability density function of absorbed radiation for sunlit leaves (left pane), shaded leaves (middle pane), and total leaf area (right pane) within a horizontally homogeneous canopy of $LAI = 1$. Each line corresponds to a different incoming diffuse radiation fraction. Open symbols correspond to the distribution obtained from 3D simulation. In all cases shown, the solar zenith angle was 0 (vertical), the leaf angle distribution was uniform, and $K = 0$ (isotropic incoming diffuse radiation).

between the two distributions.

The alternative method for producing the total absorption PDF based on sunlit-shaded leaf area partitioning is given in Fig. 8 for the same canopy cases as in Fig. 7. Addition of diffuse radiation shifts sunlit radiative fluxes upward, and decreases or eliminates sunlit leaves with a flux of 0. The flux distribution of shaded leaf area is simply the diffuse distribution with $R_{0,diff} = f_{diff}$. The sum of the sunlit and shaded distributions yields a similar total radiation distribution as when using the convolution method.

Patterns in agreement between theoretical and 3D simulated direct and diffuse distributions follow those that were separately observed for direct and diffuse radiation. Recalling that agreement for the direct distribution was excellent in all cases, and that there was small disagreement for the diffuse distribution, errors in the total distribution increased slightly with increasing $f_{diff}$ because this increases the weighting toward the diffuse distribution.

## 5. Conclusion

The theory presented in this work for determination of the probability distribution of absorbed direct, diffuse, and scattered radiation in homogeneous canopies was in close agreement with distributions obtained from 3D, leaf-resolving simulations. This not only confirmed the theory, but also verified the robustness of the 3D model. Results provided a depiction of how canopy structure affects the probability distribution of absorbed radiation, which is generally inaccessible using traditional turbid media models. Knowledge of the probability distribution of absorbed radiation fluxes in addition to volume-averaged fluxes has the potential to shed new light on interactions between plant structure and function. Although not explicitly explored in this work, these radiation distributions can serve as inputs to radiation-dependent models such as photosynthesis to understand their distribution and how it is affected by canopy structure, and potentially provide a

means for better describing the distribution of model input parameters. Future work will focus on utilizing the theory presented herein to develop schemes for simple up-scaling of processes like photosynthesis in order to efficiently predict their average values and distributions across large spatial scales. Additionally, the theory may not be valid for very tall canopies with small leaves (e.g., coniferous forests) in which penumbral effects may be important, and thus future work is needed to extend the analysis to non-collimated direct radiation.

Rigorous validation of 3D, leaf-resolving models is extremely challenging because usually only aggregate, large-scale measurements of light interception are available, which do not fully test model validity. "Exact" theoretical fluxes of absorbed radiation are available for evaluation of higher-order models, but they are typically limited to average fluxes (first order statistics) in horizontally homogeneous canopies. Comparison of 3D model outputs against the theoretical probability distributions introduced in this work can serve as what is perhaps the most rigorous theoretical test of leaf-resolving radiation absorption models currently available. Further validation work is needed to evaluate the implications of the assumptions used to derive the absorption PDF across a range of different canopy architectures. Since accomplishing this based on direct experimental data would be difficult for the reasons discussed previously, this is most likely to be done based on additional model comparisons. This could be achieved using Helios by altering settings to simulate more realistic physical conditions, by comparing against other 3D models utilizing independent assumptions or approaches, or by engaging in radiation model intercomparison exercises (e.g., Widlowski et al., 2013).

## Declaration of Competing Interest

The authors declare that they have no known competing financial interests or personal relationships that could have appeared to influence the work reported in this paper.

## Acknowledgments

This work was financially support by the USDA National Institute of Food and Agriculture, Hatch project number 1013396, and U.S. National Science Foundation grant IOS 2047628.

## Appendix A. Profile of scattered radiation intensity

For a non-emitting homogeneous medium of vegetation (such as in the solar bands), and assuming the leaf angle distribution and surface radiative properties are spatially homogeneous, the radiative transfer equation is given by Modest (2013)

$$\frac{dI(L;\boldsymbol{\Omega})}{dL}\cos\theta = -G(\boldsymbol{\Omega})\,I(L;\boldsymbol{\Omega}) + \frac{1}{\pi}\int_0^{2\pi}\int_0^{\pi}\Gamma(\boldsymbol{\Omega},\boldsymbol{\Omega}')I(L;\boldsymbol{\Omega}')\sin\theta'\,d\theta'\,d\phi', \tag{A.1}$$

where $I$ is the radiation intensity propagating along direction $\boldsymbol{\Omega}$, which has a corresponding zenith angle of $\theta$, $\boldsymbol{\Omega}'$ is the direction of scattered radiation, $L$ is the cumulative leaf area index along the vertical component of radiation propagation, and $\Gamma(\boldsymbol{\Omega},\boldsymbol{\Omega}')$ is the area scattering phase function (Myneni et al., 1988b), which is defined as

$$\Gamma(\boldsymbol{\Omega},\boldsymbol{\Omega}') = \frac{1}{2\pi}\int_0^{2\pi}\int_0^{\pi}\omega\, g_L(\boldsymbol{\Omega}_L)|\boldsymbol{\Omega}_L\cdot\boldsymbol{\Omega}||\boldsymbol{\Omega}_L\cdot\boldsymbol{\Omega}'|\,d\theta_L\,d\phi_L, \tag{A.2}$$

where

$$\omega = \begin{cases}\rho_L & \text{if } (\boldsymbol{\Omega}_L\cdot\boldsymbol{\Omega})(\boldsymbol{\Omega}_L\cdot\boldsymbol{\Omega}') > 0,\\ \tau_L & \text{if } (\boldsymbol{\Omega}_L\cdot\boldsymbol{\Omega})(\boldsymbol{\Omega}_L\cdot\boldsymbol{\Omega}') < 0,\end{cases} \tag{A.3}$$

and $\rho_L$ and $\tau_L$ are respectively the leaf reflectivity and transmissivity integrated across the radiative band of interest, and it is noted that surface reflection has been assumed to be Lambertian. It is also noted that for downwelling radiation (i.e., $\theta > \pi/2$) $L$ is zero at the canopy top and increases downward, whereas for upwelling radiation (i.e., $\theta \le \pi/2$) $L$ is zero at the ground and increases upward.

The upper boundary condition is specified based on the unobstructed downwelling solar radiation flux, which corresponds to $\theta > \pi/2$. The lower boundary condition is specified based on the properties of the ground. If the ground is black, the boundary condition at the canopy bottom is $I(0,\theta \le \pi/2) = 0$. If the ground reflects incoming radiation, the upwelling radiation at the ground $I(0,\theta \le \pi/2)$ is specified based on the downwelling intensity at the canopy bottom $I(0,\theta > \pi/2)$ and the radiative properties of the ground.

Eq. (A.1) can be integrated across space and direction using any number of numerical integration methods (e.g., trapezoidal rule, Gaussian quadrature; Press et al., 2007). For simplicity, and because computational efficiency is not an issue in the present application, a forward Euler scheme was used to integrate over the spatial dimension (i.e., $L$) and the midpoint rule was used for angular integration. If computational efficiency is important, it is suggested to use a more sophisticated scheme such as Gaussian quadrature (i.e., discrete ordinates; Myneni et al., 1988a).

Eq. (A.1) can then be solved numerically by first guessing an initial distribution for $I(L,\theta)$, then evaluating angular integrals numerically and iterating to convergence. Code for performing this solution is given in the manuscript's supplementary material.

The scattered component of the radiative intensity $I_s$ is simply given by the scattering source term in Eq. (A.1)

$$I_s(L;\boldsymbol{\Omega}) = \frac{1}{\pi}\int_0^{2\pi}\int_0^{\pi}\Gamma(\boldsymbol{\Omega},\boldsymbol{\Omega}')I(L;\boldsymbol{\Omega}')\sin\theta'\,d\theta'\,d\phi'. \tag{A.4}$$

The absorbed scattered radiation flux field $R_L$ absorbed by a leaf oriented at $\boldsymbol{\Omega}_L$ is then

$$R_L(L;\boldsymbol{\Omega}_L) = \frac{(1-\tau_L-\rho_L)}{2\pi}\int_0^{2\pi}\int_0^{\pi} I_s(L;\boldsymbol{\Omega})\,|\boldsymbol{\Omega}\cdot\boldsymbol{\Omega}_L|\cos\theta_s\sin\theta\,d\theta\,d\phi, \tag{A.5}$$

where $\theta_s$ is the solar zenith angle.

## References


Bailey, B., Kent, E., 2021. On the resolution requirements for accurately representing interactions between plant canopy structure and function in three-dimensional leaf-resolving models. In Silico Plants 3, 1–10.

Bailey, B.N., 2018. A reverse ray-tracing method for modelling the net radiative flux in leaf-resolving plant canopy simulations. Ecol. Model. 398, 233–245.

Bailey, B.N., 2019. Helios: a scalable 3D plant and environmental biophysical modelling framework. Front. Plant Sci. 10, 1185.

Bailey, B.N., Ponce de León, M.A., Krayenhoff, E.S., 2020. One-dimensional models of radiation transfer in heterogeneous canopies: a review, re-evaluation, and improved model. Geosci. Model Dev. 13, 4789–4808.

Bailey, B.N., Overby, M., Willemsen, P., Pardyjak, E.R., Mahaffee, W.F., Stoll, R., 2014. A scalable plant-resolving radiative transfer model based on optimized GPU ray tracing. Agric. For. Meteorol. 198–199, 192–208.

Baldocchi, D., Hutchison, B., Matt, D., McMillen, R., 1986. Seasonal variation in the statistics of photosynthetically active radiation penetration in an oak-hickory forest. Agric. For. Meteorol. 36, 343–361.

Bonan, G.B., Levis, S., Sitch, S., Vertenstein, M., Oleson, K.W., 2003. A dynamic global vegetation model for use with climate models: concepts and description of simulated vegetation dynamics. Global Change Biol. 9, 1543–1566.

Bonan, G.B., Patton, E.G., Finnigan, J.J., Baldocchi, D.D., Harman, I.N., 2021. Moving beyond the incorrect but useful paradigm: reevaluating big-leaf and multilayer plant canopies to model biosphere-atmosphere fluxes—A review. Agric. For. Meteorol. 306, 108435.

Campbell, G.S., 1986. Extinction coefficients for radiation in plant canopies calculated using an ellipsoidal leaf inclination distribution. Agric. For. Meteorol. 36, 317–321.

Cescatti, A., 1997. Modelling radiative transfer in discontinuous canopies of asymmetric crowns. I. Model structure and algorithms. Ecol. Model. 101, 263–274.

Chelle, M., Andrieu, B., 1998. The nested radiosity model for the distribution of light within plant canopies. Ecol. Model. 111, 75–91.

Chen, J.M., Black, T.A., 1993. Effects of clumping on estimates of stand leaf area index using the LI-COR LAI-2000. Can. J. For. Res. 23, 1940–1943.

Cieslak, M., Lemieux, C., Hanan, J., Prusinkiewicz, P., 2008. Quasi-Monte Carlo simulation of the light environment of plants. Funct. Plant Biol. 35, 837–849.

DePury, D.G.G., Farquhar, G.D., 1997. Simple scaling of photosynthesis from leaves to canopies without the errors of big-leaf models. Plant Cell Environ. 20, 537–557.

Giuliani, R., Magnanini, E., Fragassa, C., Nerozzi, F., 2000. Ground monitoring the light–shadow windows of a tree canopy to yield canopy light interception and morphological traits. Plant Cell Environ. 23, 783–796.

Goel, N.S., Strebel, D.E., 1984. Simple beta distribution representation of leaf orientation in vegetation canopies. Agron. J. 76, 800–802.

Goudriaan, J., 1977. Crop Micrometeorology: A Simulation Study. Cent. for Agric. Publ. Doc., Wageningen, Netherlands.

Harrison, A.W., Coombes, C.A., 1988. Angular distribution of clear sky short wavelength radiance. Sol. Energy 40, 57–63.

Jones, H.G., Leinonen, I., 2003. Thermal imaging for the study of plant water relations. J. Agric. Meteorol. 59, 205–217.

Jones, H.G., Vaughan, R.A., 2010. Remote Sensing of Vegetation: Principles, Techniques, and Applications. Oxford University Press, Oxford, UK, p. 400.

Keating, B.A., Carberry, P.S., Hammer, G.L., Probert, M.E., Robertson, M.J., Holzworth, D., Huth, N.I., Hargreaves, J.N.G., Meinke, H., Hochman, Z., McLean, G., Verburg, K., Snow, V., Dimes, J.P., Silburn, M., Wang, E., Brown, S., Bristow, K.L., Asseng, S., Chapman, S., McCown, R.L., Freebairn, D.M., Smith, C.J., 2003. An overview of APSIM, a model designed for farming systems simulation. Eur. J. Agron. 18, 267–288.

Kimes, D.S., Kirchner, J.A., 1982. Radiative transfer model for heterogeneous 3-D scenes. Appl. Opt. 21, 4119–4129.

Krinner, G., Viovy, N., de Noblet-Ducoudré, N., Ogée, J., Polcher, J., Friedlingstein, P., Ciais, P., Sitch, S., Prentice, I.C., 2005. A dynamic global vegetation model for studies of the coupled atmosphere-biosphere system. Global Biogeochem. Cycles 19, GB1015.

Lawrence, D., Fisher, R., Koven, C., Oleson, K., Swenson, S., Vertenstein, M., 2019. CLM5 documentation. Technical Report. National Center for Atmospheric Research..

Modest, M.F., 2013. Radiative Heat Transfer, third ed. Academic Press, Waltham, MA, p. 904.

Monsi, M., Saeki, T., 1953. Uber de lichtfaktor in de pflanzengesellschaften und seine bedeutung fur die stoffproduktion. Jpn. J. Bot. 14, 22–52.

Monsi, M., Saeki, T., 2005. On the factor light in plant communities and its importance for matter production. Ann. Bot. 95, 549.

Myneni, R., Gutschick, V., Asrar, G., Kanemasu, E., 1988a. Photon transport in vegetation canopies with anisotropic scattering Part II. Discrete-ordinates/exact-kernel technique for one-angle photon transport in slab geometry. Agric. For. Meteorol. 42, 17–40.

Myneni, R.B., Gutschick, V.P., Asrar, G., Kanemasu, E.T., 1988b. Photon transport in vegetation canopies with anisotropic scattering Part I. Scattering phase functions in one angle. Agric. For. Meteorol. 42, 1–16.

Norman, J.M., 1979. Modelling the complete crop canopy. In: Barfield, B.J., Gerber, J.F. (Eds.), Modification of the Aerial Environment of Plants. American Society of Agricultural Engineers, St. Joseph, Michigan, pp. 249–277.

Press, W.H., Teukolsky, S.A., Vetterling, W.T., Flannery, B.P., 2007. Numerical Recipes: The Art of Scientific Computing. Cambridge University Press, Cambridge, U.K., p. 1256

Pyles, R.D., Weare, B.C., Pawu, K.T., 2000. The UCD advanced canopy-atmosphere-soil algorithm: comparisons with observations from different climate and vegetation regimes. Q.J.R. Meteorol. Soc. 126, 2951–2980.

Ross, J., 1981. The Radiation Regime and Architecture of Plant Stands. Dr. W. Junk Publishers, The Hague, The Netherlands, p. 424.

Ross, J., Sulev, M., Saarelaid, P., 1998. Statistical treatment of the par variability and its application to willow coppice. Agric. For. Meteorol. 91, 1–21.

Sellers, P.J., Randall, D.A., Collatz, G.J., Berry, J.A., Field, C.B., Dazlich, D.A., Zhang, C., Collelo, G.D., Bounoua, L., 1996. A revised land surface parameterization (SiB2) for atmospheric GCMs. Part I: model formulation. J. Clim. 9, 676–705.

Sinoquet, H., Le Roux, X., Adam, B., Ameglio, T., Daudet, F.A., 2001. RATP: a model for simulating the spatial distribution of radiation absorption, transpiration and photosynthesis within canopies: application to an isolated tree crown. Plant Cell Environ. 24, 395–406.

Stenberg, P., 1995. Penumbra in within-shoot and between-shoot shading in conifers and its significance for photosynthesis. Ecol. Model. 77, 215–231.

Vesala, T., Markkanen, T., Palva, L., Siivola, E., Palmroth, S., Hari, P., 2000. Effect of variations of PAR on $CO_2$ exchange estimation for Scots pine. Agric. For. Meteorol. 100, 337–347.

Wang, Y.P., Jarvis, P.G., 1990. Description and validation of an array model - MAESTRO. Agric. For. Meteorol. 51, 257–280.

Wang, Y.P., Leuning, R., 1998. A two-leaf model for canopy conductance, photosynthesis and partitioning of available energy I: model description and comparison with a multi-layered model. Agric. For. Meteorol. 91, 89–111.

Widlowski, J.L., Pinty, B., Lopatka, M., Atzberger, C., Buzica, D., Chelle, M., Disney, M., Gastellu-Etchegorry, J.P., Gerboles, M., Gobron, N., Grau, E., Huang, H., Kallel, A., Kobayashi, H., Lewis, P.E., Qin, W., Schlerf, M., Stuckens, J., Xie, D., 2013. The fourth radiation transfer model intercomparison (RAMI-IV): proficiency testing of canopy reflectance models with ISO-13528. J. Geophys. Res. 118, 6869–6890.

de Wit, C.T., 1965. Photosynthesis of Leaf Canopies. Agricultural Research Report Wageningen.